band electrons previously described in Subsection 4.3.4.3. It occurs with the $M_{2,3}$ level for the first transition series, with the $N_{2,3}$ level for the second series (for example, strontium in Fig. 4.3.4.23) or with the $O_{2,3}$ level for the third series, including the rare-earth elements. The shape varies gradually from a plasmon-like peak with a short lifetime to an asymmetric Fano-type profile, a consequence of the coupling between discrete and continuum final states of the same energy (Fano, 1961).

4.3.4.4.2. *Bethe theory for inelastic scattering by an isolated atom (Bethe, 1930; Inokuti, 1971, 1979)*

As a consequence of the atomic nature of the excited wavefunction in core-loss spectroscopy, the first step involves deriving a useful theoretical expression for inelastic scattering by an isolated atom. The differential cross section for an electron of wavevector $\mathbf{k}$ to be scattered into a final plane wave of vector $\mathbf{k}'$, while promoting one atomic electron from ψ_0 to ψ_n, is given in a one-electron excitation description by

$$\frac{\mathrm{d}\sigma_n}{\mathrm{d}\Omega\,\mathrm{d}(\Delta E)} = \left(\frac{m_0}{2\pi\hbar^2}\right)^2 \frac{k'}{k} |\langle \psi_n \mathbf{k}' | V(\mathbf{r}) | \psi_0 \mathbf{k} \rangle|^2; \qquad (4.3.4.38)$$

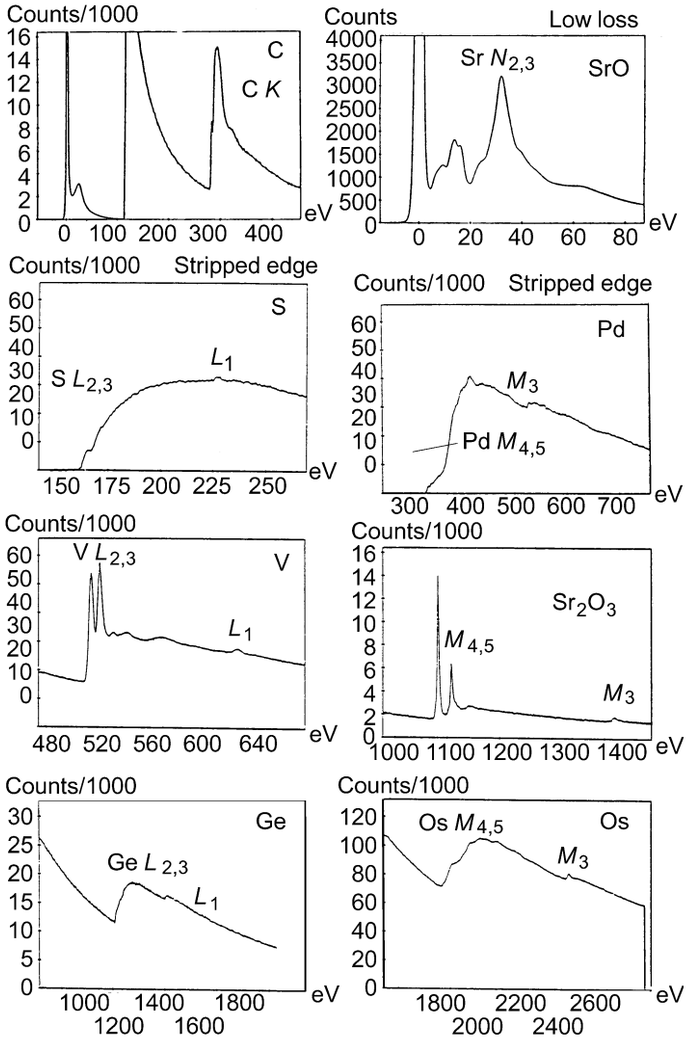

Fig. 4.3.4.23. A selection of typical profiles ($K, L_{2,3}, M_{4,5}$, and $N_{2,3}$) illustrating the most important behaviours encountered on major edges through the Periodic Table. A few edges are displayed prior to and others after background stripping. [Data extracted from Ahn & Krivanek (1982).]

see, for instance, Landau & Lifchitz (1966) and Mott & Massey (1952). The potential $V(\mathbf{r})$ corresponds to the Coulomb interaction with all charges (both in the nucleus and in the electron cloud) of the atom. The momentum change in the scattering event is $\hbar\mathbf{q} = \hbar(\mathbf{k} - \mathbf{k}')$. The final-state wavefunction is normalized per unit energy range. The orthogonality between initial- and final-state wavefunctions restricts the inelastic scattering to the only interactions with atomic electrons:

$$\frac{\mathrm{d}\sigma_n}{\mathrm{d}\Omega\,\mathrm{d}(\Delta E)} = \frac{4\gamma^2}{a_0^2 q^4} \frac{k'}{k} |\mathscr{E}_n(\mathbf{q}, \Delta E)|^2. \qquad (4.3.4.39)$$

The first part of the above expression has the form of Rutherford scattering. γ is introduced to deal, to a first approximation, with relativistic effects. The ratio k'/k is generally assumed to be equal to unity. This kinematic scattering factor is modified by the second term, or matrix element, which describes the response of the atomic electrons:

$$\mathscr{E}_n(\mathbf{q}, \Delta E) = \left\langle \psi_n \left| \sum_j \exp(i\mathbf{q}\cdot\mathbf{r}_j) \right| \psi_0 \right\rangle, \qquad (4.3.4.40)$$

where the sum extends over all atomic electrons at positions $\mathbf{r}_j$. The dimensionless quantity is known as the *inelastic form factor*.

For a more direct comparison with photoabsorption measurements, one introduces the generalized oscillator strength (GOS) as

$$\frac{\mathrm{d}f(\mathbf{q}, \Delta E)}{\mathrm{d}(\Delta E)} = \frac{\Delta E}{R} \frac{|\mathscr{E}_n(\mathbf{q}, \Delta E)|^2}{(qa_0)^2} \qquad (4.3.4.41)$$

for transitions towards final states ψ_ε in the continuum [ΔE is then the energy difference between the core level and the final state of kinetic energy ε above the Fermi level, scaled in energy to the Rydberg energy (R)]. Also,

$$f_n(\mathbf{q}) = \frac{E_n}{R} \frac{|\mathscr{E}_n(\mathbf{q})|^2}{(qa_0)^2} \qquad (4.3.4.42)$$

for transition towards bound states. In this case, E_n is the energy difference between the two states involved.

The generalized oscillator strength is a function of both the energy ΔE and the momentum $\hbar\mathbf{q}$ transferred to the atom. It is displayed as a three-dimensional surface known as the Bethe surface (Fig. 4.3.4.24), which embodies all information concerning the inelastic scattering of charged particles by atoms. The angular dependence of the cross section is proportional to

$$\frac{1}{q^2} \frac{\mathrm{d}f(\mathbf{q}, \Delta E)}{\mathrm{d}(\Delta E)}$$

at a given energy loss ΔE.

In the small-angle limit ($qr_c \ll 1$, where r_c is the average radius of the initial orbital), the GOS reduces to the optical oscillator strength

$$\frac{\mathrm{d}f(\mathbf{q}, \Delta E)}{\mathrm{d}(\Delta E)} \rightarrow \frac{\mathrm{d}f(0, \Delta E)}{\mathrm{d}(\Delta E)}$$

and

$$\mathscr{E}_n(\mathbf{q}, \Delta E) \rightarrow \mathscr{E}_n(0, \Delta E) = q^2 \left| \left\langle \psi_n \left| \sum_j \mathbf{u}\cdot\mathbf{r}_j \right| \psi_0 \right\rangle \right|^2, \qquad (4.3.4.43)$$

where $\mathbf{u}$ is the unit vector in the $\mathbf{q}$ direction. When one is concerned with a given orbital excitation, the sum over $\mathbf{r}_j$ reduces to a single term $\mathbf{r}$ for this electron. With some elementary calculations, the resulting cross section is

$$\frac{\mathrm{d}^2\sigma}{\mathrm{d}\Omega\,\mathrm{d}(\Delta E)} = \frac{4\gamma^2 R}{\Delta E\,k^2}\,\frac{1}{\theta^2+\theta_E^2}\,\frac{\mathrm{d}f(0,\Delta E)}{\mathrm{d}(\Delta E)}. \qquad (4.3.4.44)$$

The major angular dependence is contained, as in the low-loss domain, in the Lorentzian factor $(\theta^2+\theta_E^2)^{-1}$, with the characteristic inelastic angle θ_E being again equal to $\Delta E/\gamma m_0 v^2$. Over this reduced scattering-angle domain, known as the dipole region, the GOS is approximately constant and the inner-shell EELS spectrum is directly proportional to the photoabsorption cross section σ_{opt}, whose data can be used to test the results of single-atom calculations. For larger scattering angles, Fig. 4.3.4.24 exhibits two distinct behaviours for energy losses just above the edge ($\mathrm{d}f/\mathrm{d}\Delta E$ drops regularly to zero), and for energy losses much greater than the core-edge threshold. In the latter case, the oscillator strength is mostly concentrated in the Bethe ridge, the maximum of which occurs for:

$$\left.\begin{aligned}(qa_0)^2 &= \frac{\Delta E}{R} \quad \text{(non-relativistic formula)},\\ (qa_0)^2 &= \frac{\Delta E}{R}\frac{(\Delta E)^2}{2m_0c^2R} \quad \text{(relativistic formula)}.\end{aligned}\right\} \qquad (4.3.4.45)$$

This contribution at large scattering angles is equivalent to direct knock-on collisions of free electrons, *i.e.* to the curve $\Delta E = \hbar^2 q^2/2m_0$ lying in the middle of the valence-electron–hole excitations continuum (see Fig. 4.3.4.13). The non-zero width of the Bethe ridge can be used as an electron Compton profile to analyse the momentum distribution of the atomic electrons [see also §4.3.4.4.4(*c*)].

The energy dependence of the cross section, responsible for the various edge shapes discussed in §4.3.4.4.1, is governed by

$$\frac{1}{\Delta E}\,\frac{\mathrm{d}f(\mathbf{q},\Delta E)}{\mathrm{d}(\Delta E)},$$

i.e. it corresponds to sections through the Bethe surface at constant $\mathbf{q}$. Within the general theory described above, various models have been developed for practical calculations of energy differential cross sections.

The hydrogenic model due to Egerton (1979) is an extension of the quantum-mechanical calculations for a hydrogen atom to inner-shell electron excitations in an atom Z by introduction of some useful parametrization (effective nuclear charge, effective threshold energy). It is applied in practice for K and $L_{2,3}$ shells.

In the Hartree–Slater (or Dirac–Slater) description, one calculates the final continuum-state wavefunction in a self-consistent central field atomic potential (Leapman, Rez & Mayers, 1980; Rez, 1989). The radial dependence of these wavefunctions is given by the solution of a Schrödinger equation with an effective potential:

$$V_{\mathrm{eff}}(r) = V(r) + \frac{l'(l'+1)\hbar^2}{2m_0r^2}, \qquad (4.3.4.46)$$

where $[l'(l'+1)\hbar^2]/2m_0r^2$ is the centrifugal potential, which is important for explaining the occurrence of delayed maxima in spectra involving final states of higher l'. This approach is now useful for any major K, $L_{2,3}$, $M_{4,5}$, ... edge, as illustrated by Ahn & Rez (1985) and more specifically in rare-earth elements by Manoubi, Rez & Colliex (1989).

These differential cross sections can be integrated over the relevant angular and energy domains to provide data comparable with experimental measurements. In practice, one records the energy spectral distribution of electrons scattered into all angles up to the acceptance value β of the collection aperture. The integration has therefore to be made from $q_{\min} \simeq k\theta_E$ for the zero scattering-angle limit, up to $q_{\max} \simeq k\beta$. Fig. 4.3.4.25 shows how such calculated profiles can be used for fitting experimental data.

Setting $\beta = \pi$ [or equal to an effective upper limit $\theta_{\max} \simeq (\Delta E/E_0)^{1/2}$ corresponding to the criterion $q_{\max}r \simeq 1$], the integral cross section is the total cross section for the excitation of a given core level. These ionization cross sections are required for quantification in all analytical techniques using core-level excitations and de-excitations, such as EELS, Auger electron spectroscopy, and X-ray microanalysis (see Powell, 1976, 1984). A convenient way of comparing total cross sections is to rewrite the Bethe asymptotic cross section as

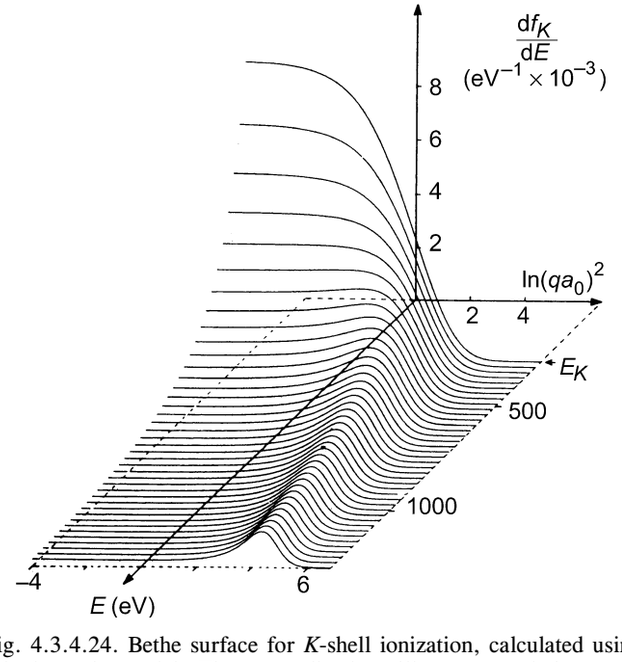

Fig. 4.3.4.24. Bethe surface for K-shell ionization, calculated using a hydrogenic model. The generalized oscillator strength is zero for energy loss E below the threshold E_K. The horizontal coordinate is related to scattering angle through q [from Egerton (1979)].

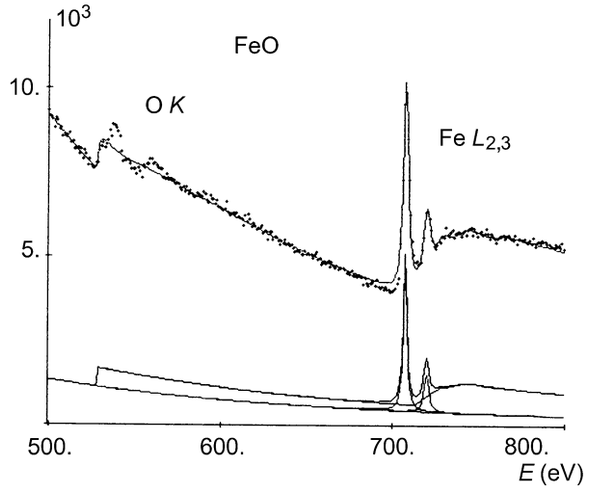

Fig. 4.3.4.25. A novel technique for simulating an energy-loss spectrum with two distinct edges as a superposition of theoretical contributions (hydrogenic saw-tooth for O K, Lorentzian white lines and delayed continuum for Fe $L_{2,3}$ calculated with the Hartree–Slater description). The best fit between the experimental and the simulated spectra is shown; it can be used to evaluate the relative concentration of the two elements [see Manoubi *et al.* (1990)].

$$\sigma_{nl}E_{nl}^2 = 6.51 \times 10^{-14}\, Z_{nl} b_{nl} \frac{\log(C_{nl}U_{nl})}{U_{nl}}, \qquad (4.3.4.47)$$

when the result is given in cm^2, σ_{nl} is the total cross section per atom or molecule or ionization of the *nl* subshell with edge energy E_{nl}, Z_{nl} is the number of electrons on the *nl* level, and U_{nl} is the overvoltage defined as E_0/E_{nl}. b_{nl} and c_{nl} are two parameters representing phenomenologically the average number of electrons involved in the excitation and their average energy loss (one finds for the major K and $L_{2,3}$ edges $b_{nl} \simeq 0.6$–0.9 and $c_{nl} \simeq 0.5$–0.7). These values are in practice estimated from plots of curves $\sigma_{nl}E_{nl}^2U_{nl}$ as a function of $\log U_{nl}$, known as Fano plots. From least-squares fits to linear regions, one can evaluate the values of b_{nl} (slope of the curves) and of $\log c_{nl}$ (coordinate at the origin) for various elements and shells. However, it has been shown more recently (Powell, 1989) that the interpretation of Fano plots is not always simple, since they typically display two linear regions. It is only in the linear region for the higher incident energies that the plots show the asymptotic Bethe dependence with the slope directly related to the optical data. At lower incident energies, another linear region is found with a slope typically 10–20% greater. Despite great progress over the last two decades, more cross-section data, either theoretical or experimental, are still required to improve to the 1% level the accuracy in all techniques using these signals.

4.3.4.4.3. *Solid-state effects*

The characteristic core edges recorded from solid specimens display complex structures different from those described in atomic terms. Moreover, their detailed spectral distributions depend on the type of compound in which the element is present (Leapman, Grunes & Fejes, 1982; Grunes, Leapman, Wilker, Hoffmann & Kunz, 1982; Colliex, Manoubi, Gasgnier & Brown, 1985). Modifications induced by the local solid-state environment concern (see Fig. 4.3.4.26) the following:

(*a*) *The threshold* (or edge itself), which may vary in position, slope, and associated fine structures. From photoelectron spectroscopies (UPS, XPS), an edge displacement along the energy scale is known as a 'chemical shift': it is due to a shift in the energy of the initial level as a consequence of the atomic potential modifications induced by valence-electron charge transfer (*e.g.* from metal to oxide). EELS is actually a two-level spectroscopy and the observed changes at edge onset concern both initial and final states. Consequently, measured shifts are due to a combination of core-level energy shift with bandgap and exciton creation. Some important shifts have been measured in EELS such as:

– carbon K: 284 to 288 eV from graphite to diamond;

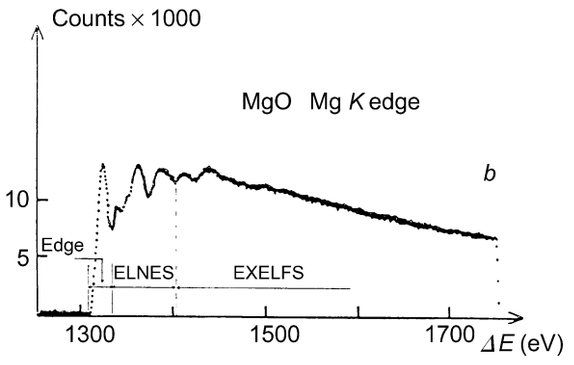

Fig. 4.3.4.26. Definition of the different fine structures visible on a core-loss edge.

– aluminium $L_{2,3}$: 73 to 77 eV from metal to Al_2O_3;

– silicon $L_{2,3}$: 99.5 to 106 eV from Si to SiO_2.

However, 'chemical shift' constitutes a simplified description of the more complex changes that may occur at a given threshold in various compounds. It assumes a rigid translation of the edge, but in most cases the onset changes in shape and there are no simple features to correlate through the different spectra. This remark is more relevant with the increased energy resolution that is now available. With a sub-eV value, extra peaks or splittings can frequently be detected on edges that exhibit simple shapes when recorded at lower resolution. Among others, the L_{32} white lines in transition metals show different behaviours when involved in various environments:

– crystal-field-induced splitting for each line in the oxides Sc_2O_3, TiO_2 when compared with the metal (see Fig. 4.3.4.27).

– relative change in L_3/L_2 intensity ratio between different ionic species [most important when the occupancy degree n for the d band is of the order of 5, *i.e.* around the middle of the transition series, *e.g.* Mn and Fe oxides; see for instance, Rask, Miner & Buseck (1987) and Rao, Thomas, Williams & Sparrow (1984)].

– presence of a narrow white line instead of a hydrogenic profile when the electron transfer from the metal to its ligand induces the existence of vacant d states at the Fermi level (CuO compared with Cu, see Fig. 4.3.4.28).

(*b*) *The near-edge fine structures* (ELNES), which extend over the first 20 or 30 eV above threshold (Taftø & Zhu, 1982; Colliex *et al.*, 1985). These are very similar to XANES structures in X-ray photoabsorption spectroscopy: they mostly reflect the spectral distribution of vacant accessible levels and are consequently very sensitive to site symmetry and charge transfer. Several approaches have been proposed to interpret them. A molecular-orbital description [*e.g.* Fischer (1970) or Tossell, Vaughan & Johnson (1974)] classifies the energy levels, both occupied and unoccupied, for clusters comprising the central excited ion and its first shell of neighbours. Its major success lies in the interpretation of level splitting on edges.

A one-electron band calculation constitutes a second step with noticeable successes in the case of metals (Müller, Jepsen &

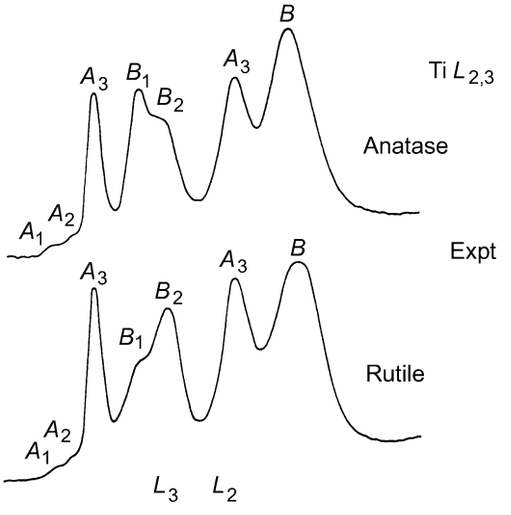

Fig. 4.3.4.27. High-energy resolution spectra on the $L_{2,3}$ titanium edge from two phases (rutile and anatase) of TiO_2. Each atomic line L_3 and L_2 is split into two components A and B by crystal-field effects. The new level of splitting B_1B_2 that distinguishes the two spectra is not yet understood. In Ti metal, the L_3 and L_2 lines are not split by structural effects [courtesy of Brydson *et al.* (1989)].

references